Physica Medica 51 (2018) 13–21

Contents lists available at ScienceDirect

Physica Medica

journal homepage: www.elsevier.com/locate/ejmp

Technical note

Physical parameter optimization scheme for radiobiological studies of charged particle therapy

Changran Geng[a,b,1], Drake Gates[c,2], Lawrence Bronk[d], Duo Ma[e], Fada Guan[e,*]

[a] Department of Nuclear Science and Engineering, Nanjing University of Aeronautics and Astronautics, Nanjing 210016, China
[b] Department of Radiation Oncology, Massachusetts General Hospital and Harvard Medical School, Boston, MA 02114, USA
[c] Orbital Debris Program Office, NASA Johnson Space Center, Houston, TX 77058, USA
[d] Department of Radiation Oncology, The University of Texas MD Anderson Cancer Center, Houston, TX 77030, USA
[e] Department of Radiation Physics, The University of Texas MD Anderson Cancer Center, Houston, TX 77030, USA

ARTICLE INFO

Keywords:
Charged particle therapy
Monte Carlo
Python
Optimization

ABSTRACT

We have developed an easy-to-implement method to optimize the spatial distribution of a desired physical quantity for charged particle therapy. The basic methodology requires finding the optimal solutions for the weights of the constituent particle beams that together form the desired spatial distribution of the specified physical quantity, e.g., dose or dose-averaged linear energy transfer (LET_d), within the target region. We selected proton, ^{4}He ion, and ^{12}C ion beams to demonstrate the feasibility and flexibility of our method. The pristine dose Bragg curves in water for all ion beams and the LET_d for proton beams were generated from Geant4 Monte Carlo simulations. The optimization algorithms were implemented using the Python programming language. High-accuracy optimization results of the spatial distribution of the desired physical quantity were then obtained for different cases. The relative difference between the real value and the expected value of a given quantity was approximately within ± 1.0% in the whole target region. The optimization examples include a flat dose spread-out Bragg peak (SOBP) for the three selected ions, an upslope dose SOBP for protons, and a downslope dose SOBP for protons. The relative difference was approximately within ± 2.0% for the case with a flat LET_d (target value = 4 keV/μm) distribution for protons. These one-dimensional optimization algorithms can be extended to two or three dimensions if the corresponding physical data are available. In addition, this physical quantity optimization strategy can be conveniently extended to encompass biological dose optimization if appropriate biophysical models are invoked.

1. Introduction

The number of proton and heavy ion therapy centers has dramatically increased in recent years around the world [1]. This can be attributed to many factors. First, from a physics perspective, the characteristics of a well-defined penetration range of ions can enable the delivery of a highly conformal dose to the tumor volumes while sparing the surrounding normal tissues [2]. In addition, for some specific disease sites, clinical trials have shown promising results in regards to the effectiveness of ion therapy compared with photon-based radiotherapy [3,4]. Moreover, the total cost of building a proton or heavy ion center keeps decreasing with the development of new techniques [5–7].

In clinical applications, a sharp dose Bragg peak from a mono-energetic ion beam is usually not wide enough to cover the volumetric target tumor. Instead, a spread-out Bragg peak (SOBP[2]) formed by multi-energetic beams with appropriate modulations can be used to cover the large volume of a tumor. An SOBP can be delivered by either passively scattered particle beams with range modulations or actively scanned beams with intensity modulations [8,9]. Nevertheless, the scanning technique is becoming routine and nearly all new particle therapy centers have been equipped with scanning nozzles because of the unique advantages it offers [9]. In a radiation field generated by scanned particle beams, the weight of each Bragg curve can be modulated to deliver a desired shape of dose distribution to the target tumor. This flexibility in dose delivery forms the physical basis for multi-field optimized intensity-modulated ion (or proton) therapy.

* Corresponding author.
E-mail address: FGuan@mdanderson.org (F. Guan).

[1] Part of this work was performed when the author was working at Massachusetts General Hospital and Harvard Medical School.

[2] Part of this work was performed when the author was working at The University of Texas MD Anderson Cancer Center.

[3] Usually, a dose SOBP refers to a uniform dose distribution longitudinally within the target, but in the current study, we do not restrict it to be a uniform dose. As long as multiple modulated beams contribute to the desired shape of the dose distribution within the target, we treat it as a dose SOBP.

https://doi.org/10.1016/j.ejmp.2018.06.001
Received 23 January 2018; Received in revised form 18 May 2018; Accepted 2 June 2018
Available online 14 June 2018

Different approaches and algorithms to optimize the spatial dose distributions of scanned particle beamlets have been developed for years [10–15]. A beam delivery strategy can be optimized using a treatment planning system (TPS) for particle therapy. However, for some radiobiologic studies, the treatment planning system may not meet all of the unique requirements for designing a cell or animal irradiation experiment. For example, a TPS is usually designed to process objects with large dimensions such as human cancer patients, and it may not be suitable to handle small geometries such as those for animals and cells. In addition, a TPS is usually limited to performing dose optimization only and may not be able to calculate other physical quantities such as linear energy transfer (LET) and particle energy spectra, which are needed to interpret the biological effects in particle radiobiology experiments. Given these limitations, it is imperative to develop a convenient and effective tool that can facilitate the use of scanned beams for particle radiobiology experiments to correlate the observed biological effects with physical parameters.

For the desired spatial distribution of a specified physical quantity, the following two steps are usually needed: (1) obtain the raw data of the physical quantity for all beams with different energies, and (2) perform the optimization procedure to solve the beam weights. In many previous studies [16–20], an analytical method was adopted to rapidly generate the Bragg curves and then the optimization procedure was performed to generate a dose SOBP. Although the analytical method has advantages in the calculation speed, systematic uncertainties exist owing to the approximated expression of Bragg peaks in the dose calculations. Using the measured data of the physical quantity may improve the accuracy of the input data for optimizations. However, in some conditions, the measured data are not easily obtained. Using benchmarked Monte Carlo systems to generate the physical data can be an effective alternative to save time in obtaining measurements while maintaining the accuracy of the optimization results.

In addition to the dose optimizations, many other respects have been optimized in charged particle therapy. For example, Dias et al. have analyzed the impact of different optimization methods in the charged particle therapy scanning paths by assessing the possibility to deflect the beam out of the extraction line during irradiation [21]. Austin et al. have developed a Monte Carlo Markov model for assisting proton therapy referral decision making [22]. Kanematsu has developed a dose calculation algorithm of fast fine-heterogeneity correction for heavy charged particle radiotherapy [23]. Trott has investigated special radiobiological features of second cancer risk after particle radiotherapy and concluded that it is unlikely that modern particle therapy has higher risk than photon therapy [24]. Bassler et al. have investigated the LET painting technique to place more high-LET particles in target tumors [25,26].

Although various approaches for optimizing particle beams have been available for years, our work has its unique novelties. First, the current study aimed to develop a general and easy-to-implement methodology to generate an optimized beam delivery strategy in terms of commonly used physical quantities such as dose and dose-averaged LET (LET_d) for radiobiological studies. In addition, the generated beam delivery plan can be applied to cell or animal experiments to investigate how the physical parameters influence the observed biological effects. Moreover, the methodology developed for physical quantity optimization can be conveniently extended to relative biological effect (RBE)-weighted dose optimization if appropriate biophysical models are invoked. The results of such efforts will be reported in future work.

2. Materials and methods

2.1. Basic settings in Monte Carlo simulations

The general-purpose Monte Carlo toolkit Geant4 [27,28] (version 10.3.p03) was used to perform the particle tracking to generate the depth dose curves for different ions and the depth LET_d curves for proton beams only. In the current work, these raw data were used as the input to the physical quantity optimization process. For charged particle therapy, various physics lists are available such as “QBBC”, “FTFP_BERT” and many others, all of which contain both of the electromagnetic and hadronic physics processes. We compared the simulation results from the above two physics lists and found the dose difference is below 1% for the selected ions within the therapeutic energy ranges. In this study, we selected the “FTFP_BERT” physics list as a representative for all the simulations as we did in our previous studies [29,30].

The 94 groups of scanned proton beams used at The University of Texas MD Anderson Proton Therapy Center were selected for the calculations. The energy varies from 72.5 to 221.8 MeV with a range (depth with 90% of the peak dose in the distal falloff) of 4.0 to 30.6 cm in water. For ^{4}He ions and ^{12}C ions, the virtual beams were modelled using energies derived from publicly available databases because our institution lacks clinical facilities that utilize heavy ions. The National Institute of Standards and Technology ASTAR [31] program was used to determine the energy and range of ^{4}He ions, and 161 groups of ^{4}He ions with energies of 70–230 MeV/n and ranges of 4.1–33.1 cm in water were selected on the basis of commonly used clinical treatment depths in patients. For ^{12}C ions, the energy and range data were obtained from the Errata and Addenda: ICRU Report 73 [32]. A total of 161 groups of energies with energies of 120 to 440 MeV/n and ranges of 3.6 to 32.0 cm in water were selected. All of the beams were assumed to have a Gaussian-shaped energy spread and a Gaussian-shaped spot profile in both of the classic x and y directions where the beam direction is assumed to be along a central z axis.

An $80 \times 80 \times 40\,cm^3$ water phantom was built as the target for scoring quantities of interest for different ion beams. A scorer with a large radius of 40 cm and thickness of 0.01 cm is built so that the simulation data with a high spatial resolution (along the z axis) could be obtained. Therefore, the scored dose can be approximately treated as the integral depth dose (IDD). Although only the simulation results along the depth were reported, the multiple Coulomb scattering processes were considered during the Monte Carlo simulations. In our radiobiology studies, a uniform radiation field at a specified depth can be easily formed by a series of equal-weight scanned beam spots with the same energy. Therefore, to form a desired 3D distribution (laterally uniform within the target) of a specified physical quantity, we only need to perform the one-dimension (depth) optimization procedure for beams with different energies. In particular, a pseudo double-layer ripple filter was modelled for carbon ions only to broaden the Bragg peak. The number of primary source particles was set as 10^7 for each beamlet to make the simulation results, e.g., total dose, meet the statistical uncertainty requirement (relative error of the mean value $<$ 1%) when the dose is larger than 5% of the peak dose. All associated simulation data were then written to ROOT histograms [33].

2.2. Dose optimization algorithm for proton and heavy ion beams

We used the Python programming language (version 3.4.3) and its NumPy and SciPy libraries to perform the physical quantity optimization procedures. The basic principle of an optimization algorithm is to find the optimal solutions for the weight of each beamlet to form the desired distribution of the specified physical quantity within the target, using an iterative scheme.

For dose optimization procedures, only the IDDs of all beamlets are needed, and these were generated from the Monte Carlo simulations. Initially, the IDD data are read into the Python program and each IDD is then normalized by its peak dose. Therefore, we can assume the peak dose is 1.0 Gy after the normalization if we assign Gy as the dose units. The normalized IDD dataset is used in seeking the optimal solutions for the beam weights. Next, the boundaries of the target region and the corresponding target dose distribution should be specified. Assuming the expected target dose at depth z is $D_t(z)$ and the real dose after

optimization is $D_r(z)$, the relative difference between the real dose and expected dose can then be calculated using Eq. (1). This metric is defined to quantify the accuracy of the dose optimization procedure. A relative difference within ± 2.0% is treated to be acceptable after optimization in the current study.

$$\sigma_D(z) = \frac{D_r(z) - D_t(z)}{D_t(z)} \times 100\% \quad (1)$$

Dose optimization is an iterative process to find the optimal weight of each beamlet to minimize the difference between $D_r(z)$ and $D_t(z)$. In our optimization algorithm, the Python function *curve_fit()* from SciPy was selected as the optimizer to solve the beam weights using the nonlinear least-squares minimization scheme based on the Levenberg–Marquardt algorithm [34]. We set the relative error of 0.1% for $D_t(z)$ within the target to increase the importance of these data points during the data fitting. After optimization, $D_r(z)$ can be calculated using Eq. (2).

$$D_r(z) = \sum_i w_i * D_i(z) \quad (2)$$

Here w_i is the weight of the ith beamlet and $D_i(z)$ is the normalized dose at depth z in the ith beamlet's IDD curve. In the optimization process, we use Gy as the units for $D_i(z)$, $D_r(z)$, and $D_t(z)$, which means they are all expressed as absolute values. Therefore, the weight of each beamlet is also an absolute value and thus is not required to make the sum of w_i unity.

In the optimization process, only the beamlets with penetration ranges that can cover the target region are considered when finding the beam weights; for the outlier energy groups, the weight is directly set to a very small value, i.e., 1.0E-10. For protons, as an example, if we assume the target region is 5 to 10 cm, we need only to determine weights for beamlets with energies from 81.4 MeV (energy ID = 11 and range = 5.0 cm) to 118.6 MeV (energy ID = 46 and range = 10.1 cm). However, this energy-penetration range selection scheme may result in large fluctuations for the relative difference at the lower and upper boundary of the target region. We discuss this in detail in the Results.

2.3. Let_d optimization algorithm for proton beams

For proton beams, LET_d has been used as a surrogate quantity to indicate the RBE [35]. Some RBE calculation models assume a linear relationship between RBE and LET_d [36,37]. Therefore, we selected LET_d as a physical quantity of interest to perform the LET_d optimization procedure in the target region to demonstrate the flexibility of the optimization algorithms. Please note that the concept of LET_d optimization in our radiobiological studies is different from the concept of LET_d-guided dose optimization for patient treatment plans which adds LET-based objectives to maximize LET in target volumes while minimizing the LET in critical structures and normal tissues [35,38]. In the calculation of LET_d, only primary protons were included to make it consistent with the definition of LET by ICRU taking into account only the electronic interactions of primary charged particles [39]. The secondary protons generated in water are mostly from the nonelastic nuclear reactions [40], which are not described and quantified by LET [39]. For clinically heavier ion beams, LET_d is not an appropriate physical quantity because of the high heterogeneity of the radiation field in the target geometry, which is mainly composed of different types of recoil nuclei besides the primary particles. According to the definition of LET, it can be applied only to a specified type of charged particles, rather than a mixture of multiple types of charged particles. Therefore, it is inappropriate to calculate LET_d for ^{4}He and ^{12}C ion beams in the target geometry. Henceforth, we calculated LET_d only for proton beams and then performed the optimization procedure to generate a desired spatial distribution of LET_d within the target region.

The LET_d calculation method for each single proton beamlet using Geant4 has been described in our previous study [41]. Here we provide the formula to calculate LET_d from mixed proton beams after optimization, expressed in Eq. (3).

$$LET_{d,r}(z) = \frac{\sum_i w_i * D_i(z) * LET_{d,i}(z)}{\sum_i w_i * D_i(z)} \quad (3)$$

Here $LET_{d,r}(z)$ is the real LET_d at depth z, $LET_{d,i}(z)$ is the LET_d at depth z from the ith beamlet in the raw pristine LET_d dataset, w_i is the weight of the ith beamlet, $D_i(z)$ is the normalized dose at depth z in the ith beamlet's IDD curve, $w_i * D_i(z)$ is the weighted dose from the ith beamlet, and $\sum_i w_i * D_i(z)$ is the real dose at depth z after optimization. It should be noted that according to the LET_d calculation method, the dose $w_i * D_i(z)$ is the actual weighting factor for $LET_{d,i}(z)$, whereas w_i is the weighting factor for the IDD of the ith beamlet. Once LET_d optimization is complete, w_i from all beams can be solved. Then, substituting all of the w_i into Eq. (2), the real dose at depth z can be calculated.

If $LET_{d,t}(z)$ is the expected LET_d at depth z, the relative difference between the real value and the expected value can be calculated using Eq. (4).

$$\sigma_{LET_d}(z) = \frac{LET_{d,r}(z) - LET_{d,t}(z)}{LET_{d,t}(z)} \times 100\% \quad (4)$$

Similar to the dose optimization procedure, the optimization process for LET_d is to find the optimal weight of each beamlet to minimize the difference between the real and the expected LET_d value.

3. Results

First, we present the IDDs from each of the three types of ion beams and the depth LET_d curves for proton beams only. They are the basic data for the physical quantity optimizations.

Theoretically, any shape of the target dose distribution can be specified in the optimization process, but the optimizer may not find appropriate solutions for the beam weights with an acceptable accuracy, e.g., ± 2.0% of the relative difference. Below we show only results from simple and commonly used target dose distributions to demonstrate our method. Similarly, for proton LET_d optimization, we show only results from simple cases.

3.1. Physical quantities generated from Monte Carlo simulations

The 94 groups of normalized IDDs for proton beams are shown in Fig. 1A. The depth LET_d distribution of proton beams is shown in Fig. 1B. These data were generated from Geant4 Monte Carlo simulations. The LET_d for each beamlet was cut at the depth with 1% of the peak dose in the distal falloff owing to the negligible influence of protons beyond this depth.

The 161 groups of normalized IDDs of ^{4}He ion beams are shown in Fig. 2A. The 161 groups of normalized IDDs of ^{12}C ion beams are shown in Fig. 2B. The fragmentation tails distal to the Bragg peaks can be clearly observed for ^{4}He and ^{12}C ion beams. The datasets for Figs. 1 and 2 form the basis for the next step, physical quantity optimization procedures.

3.2. Flat dose SOBP of proton beams

A flat physical dose SOBP is the most commonly used dose distribution to demonstrate the physical advantage of particle therapy. In clinical proton therapy, a flat dose SOBP is often used to cover the tumor volume because the RBE is assumed to be a constant value of 1.1. For ^{4}He and ^{12}C ion therapy, the spatially varied RBE is usually taken into account; therefore, a non-flat physical dose distribution should be applied to the target region. This notwithstanding, to simplify the calculation, we specified a flat physical dose distribution in a target region

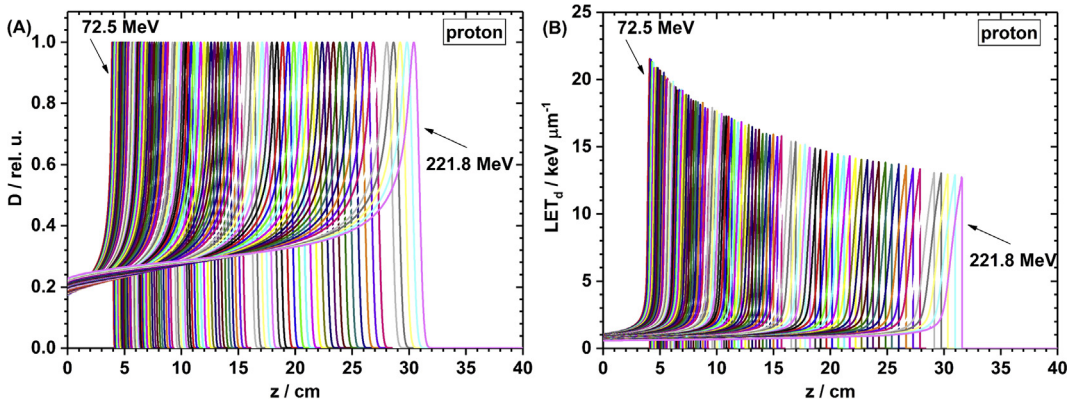

Fig. 1. (A) Integral depth dose (IDD) of 94 groups of proton beams. (B) Dose-averaged linear energy transfer (LET$_d$) of proton beams. Beyond the depth with 1% of the peak dose, the LET$_d$ value is cut.

for each of the selected ions to demonstrate our dose optimization algorithms. The target was assumed to extend from 5 to 10 cm in water and the target dose was set as 2 Gy uniformly.

We first present the optimization results from proton beams. The percent dose SOBP and its constituent weighted dose curves are depicted in Fig. 3A. The SOBP is formed by 36 beams ranging from 81.4 to 118.6 MeV, but the data from the 81.4-MeV beamlet is unseen owing to its relatively low contribution. The absolute dose (Gy) and LET$_d$ distributions are shown in Fig. 3B. The LET$_d$ ranges from 1.8 to 8.5 keV/μm from 5 to 10 cm. The relative difference between the real dose after the optimization procedure and the expected dose within the target region is shown in Fig. 3C. The relative difference varied from −2.0 to 0.5% for the whole target region, but at the central area the relative difference was much lower and nearly within ± 0.2%. In addition, we provide an example with a much smaller target region to demonstrate the flexibility of our algorithm. Fig. 3D shows the flat dose SOBP and its constituent weighted beams for a small target of 4–6 cm.

3.3. Flat dose SOBP of ^{4}He ion beams

The percent depth dose distribution from ^{4}He ions with an SOBP from 5 cm to 10 cm in water and its constituent weighted dose curves from different beams are shown in Fig. 4A and the corresponding relative differences at different locations are shown in Fig. 4B. The SOBP is formed by 39 groups of ^{4}He ion beams with energies ranging from 78.0 to 116.0 MeV/n. The data from group #9 with 78.0 MeV/n and group #46 with 115.0 MeV/n are unseen owing to the much lower beam weights. In Fig. 4B, the relative difference varies from -2.0 to 0.7% for the whole target region, but at the central area the relative difference is much lower and nearly within ± 0.1%.

3.4. Flat dose SOBP of ^{12}C ion beams

The percent depth dose distribution from ^{12}C ions with an SOBP from 5 to 10 cm in water and its constituent weighted dose curves from different beams are shown in Fig. 5A and the corresponding relative differences at different locations are shown in Fig. 5B. The SOBP is formed by 38 groups of ^{12}C ion beams with energies ranging from 150.0 to 224.0 MeV/n. The data from group #16 with 150.0 MeV/n, group #18 with 154.0 MeV/n, group #50 with 218.0 MeV/n, and group #52 with 222.0 MeV/n are unseen owing to the much lower beam weights. In Fig. 5B, the relative difference varies from -1.0 to 0.3% for the whole target region, but at the central area the relative difference is much lower and nearly within ± 0.1%.

3.5. Upslope and downslope dose distribution of protons

For multi-field intensity-modulated proton therapy, it is not necessary to apply a flat dose SOBP for each field. The superposition of non-uniform dose distributions from multiple fields can deliver a uniformly accumulated dose to the target. In the current study, we selected two simple cases to deliver intensity-modulated proton therapy by two opposed fields. In the first case, the uniform target dose was formed by two opposed upslope dose SOBPs. In the second case, the uniform target dose was formed by two opposed downslope dose SOBPs. In this section, we report the results from one upslope dose SOBP and one downslope dose SOBP.

3.5.1. Upslope dose distribution

In the case with an upslope dose SOBP (5–10 cm in water), we specified the starting and ending dose to be 0.8 and 1.2 times the dose at mid-SOBP. The optimized upslope dose SOBP and its constituent

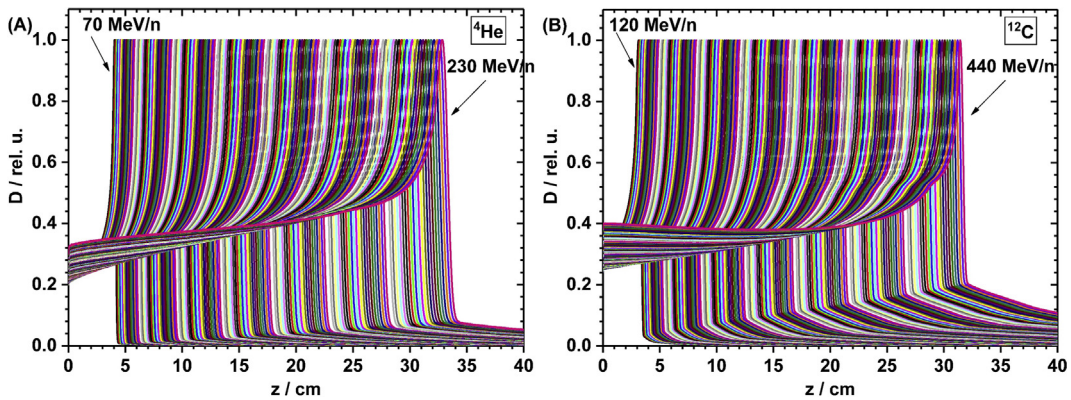

Fig. 2. (A) Integral depth dose (IDD) of 161 groups of ^{4}He ion beams. (B) IDD of 161 groups of ^{12}C ion beams.

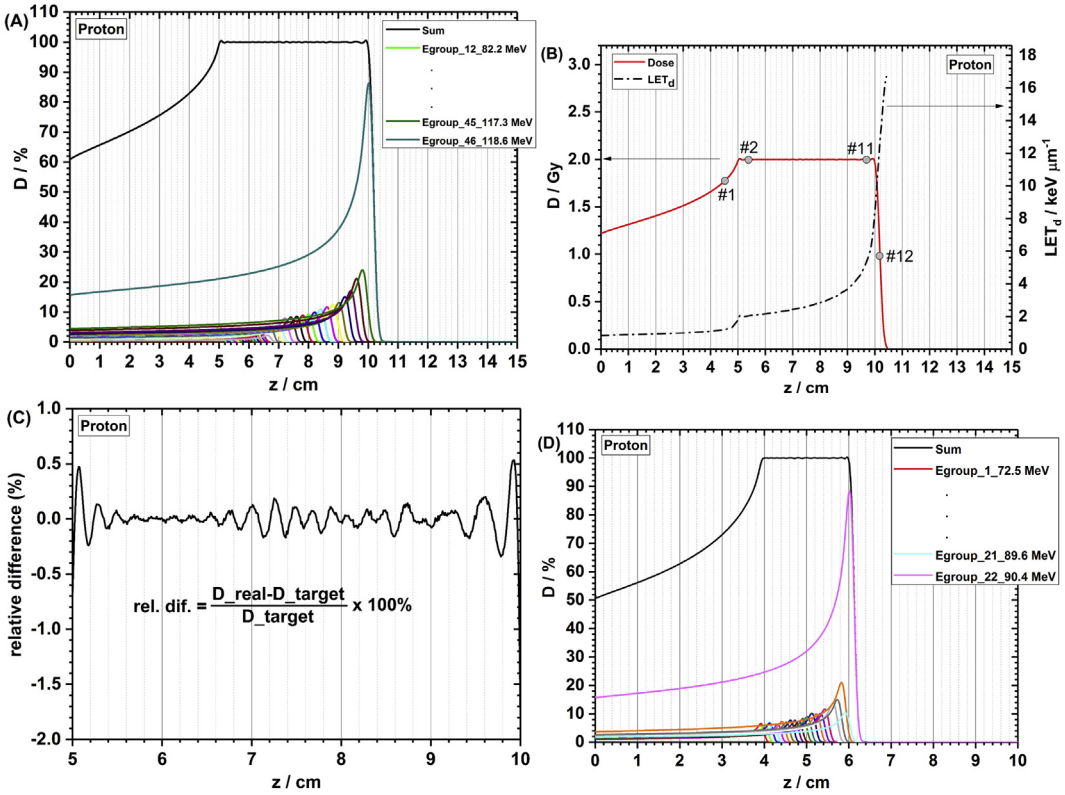

Fig. 3. (A) Flat dose spread-out Bragg peak (%) and its constituent proton beams with the target of 5–10 cm. (B) Dose (Gy) and dose-averaged linear energy transfer (LET$_d$) distributions. The labels #1 to #12 indicate the spatial locations that are selected to investigate the biological effects. (C) Relative difference between the real dose after the optimization procedure and the expected dose within the target region from 5 to 10 cm in water. (D) Flat dose spread-out Bragg peak (%) and its constituent proton beams with the target of 4–6 cm.

weighted dose curves are shown in Fig. 6A. The data from the 81.4-MeV beamlet are unseen in the dose curves owing to the relatively low contribution of this beamlet. The relative difference curve is shown in Fig. 6B. Close to the upper boundary of the SOBP with the highest dose, the relative difference fluctuated widely from −1.2% to 0.5%. For most of the other locations, the relative difference was as small as within ± 0.1%.

3.5.2. Downslope dose distribution

In the case with a downslope dose SOBP (5 to 10 cm in water), we specified the starting and ending dose to be 1.9 and 0.1 times the dose at mid-SOBP. The optimized downslope dose SOBP and its constituent weighted dose curves are shown in Fig. 7A. The data from the 81.4-MeV beamlet are unseen in the dose curves owing to the relatively low contribution of this beamlet. The relative difference curve is shown in Fig. 7B. Close to the lower boundary of the SOBP with the highest dose, the relative difference fluctuated widely from −2.7% to 1.3%. For other locations, the relative difference was within ± 0.5%.

3.6. Flat LET$_d$ distribution of protons

We have observed large fluctuations at the optimization target boundaries for the dose optimization. Here, we first report the results with an expected uniform LET$_d$ distribution within the target region from 5 to 10 cm. The expected LET$_d$ was set as 4 keV/μm. The LET$_d$ and dose curves after the LET$_d$ optimization procedure are shown in Fig. 8A. As we stated in section 2.3, dose is only a relative weighting factor for LET$_d$ optimization, so the units of dose can be arbitrary. Nevertheless,

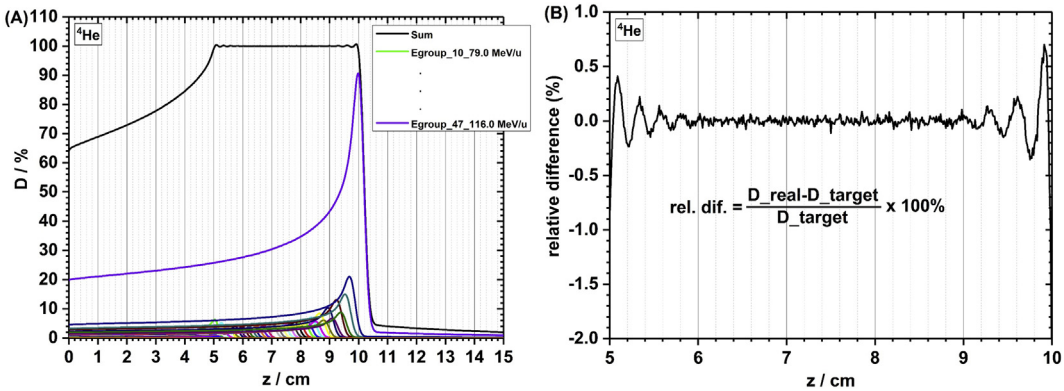

Fig. 4. (A) Flat dose spread-out Bragg peak (%) and its constituent ^{4}He ion beams. (B) Relative difference between the real dose after the optimization procedure and the expected dose within the target region from 5 to 10 cm in water.

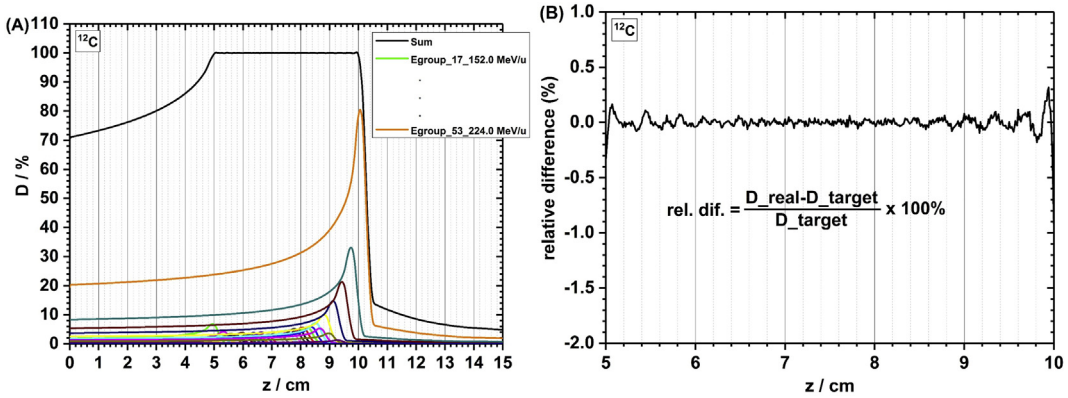

Fig. 5. (A) Flat dose spread-out Bragg peak (%) and its constituent ^{12}C ion beams. (B) Relative difference between the real dose after the optimization procedure and the expected dose within the target region from 5 to 10 cm in water.

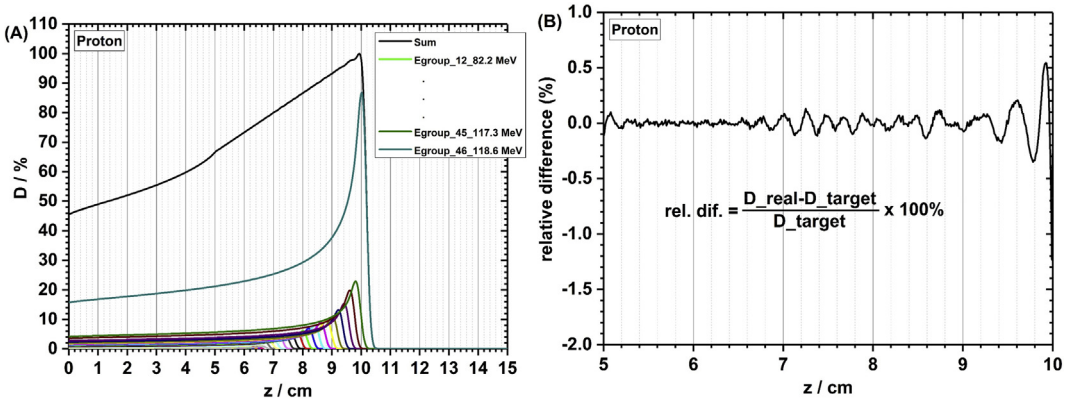

Fig. 6. (A) Proton upslope dose spread-out Bragg peak and its constituent beams. (B) Relative difference between the real dose after the optimization procedure and the expected dose within the target region from 5 to 10 cm in water.

we specified the dose at the middle of the SOBP to be 2 Gy. We can clearly observe the difference between the real LET_d and the expected value in Fig. 8A. The distribution of the relative difference for LET_d optimization is shown in Fig. 8B. The relative difference within the central area, i.e., from 5.5 to 9.5 cm, is between −2.5% and 3.5%. However, the relative difference can be as high as −17% and 88% at the lower and higher boundaries. The large difference at optimization target boundaries are due to the sharp increase of LET_d as illustrated in Fig. 3B, in which the LET_d is 1.8 and 8.5 keV/μm at 5 and 10 cm with a flat dose distribution.

To obtain high-accuracy results within the specified target area for radiobiology experiments, we extended the optimization boundary 5 mm externally on each side as a margin. For example, if the irradiation target region set in the optimization extended from 5 to 10 cm, the new optimization boundary was 4.5–10.5 cm. Here, we specify the 4.5–10.5 cm region as the optimization target while set the 5–10 cm as the irradiation target. Please note that, the "optimization target" can be different from the term of an "irradiation target" in a radiobiology experiment. As illustrated in Fig. 3B, the target cells can be sampled at any desired locations along the path of beams. Therefore, the lower and higher boundaries are used to define the optimization target for a physical quantity, rather than the irradiation target(s) used in a radiobiology study or a treatment target volume in radiotherapy.

In Fig. 9A, we can observe the flat LET_d within the irradiation target

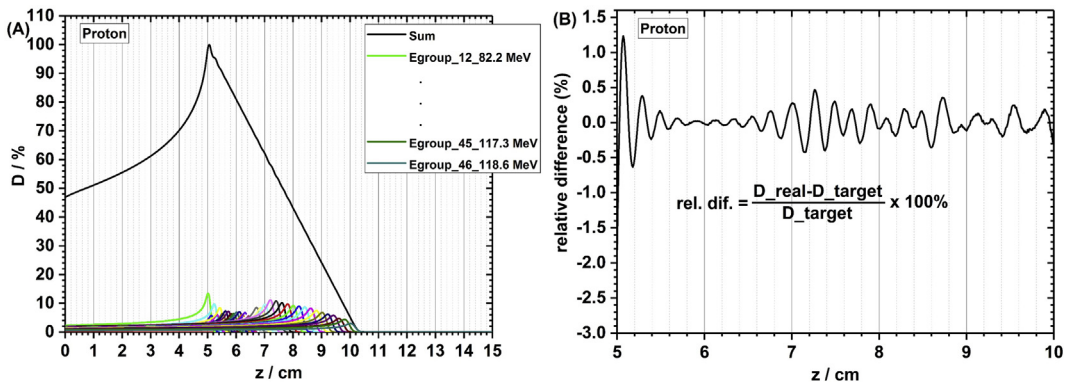

Fig. 7. (A) Proton downslope dose spread-out Bragg peak and its constituent beams. (B) Relative difference between the real dose after the optimization procedure and the expected dose within the target region from 5 to 10 cm in water.

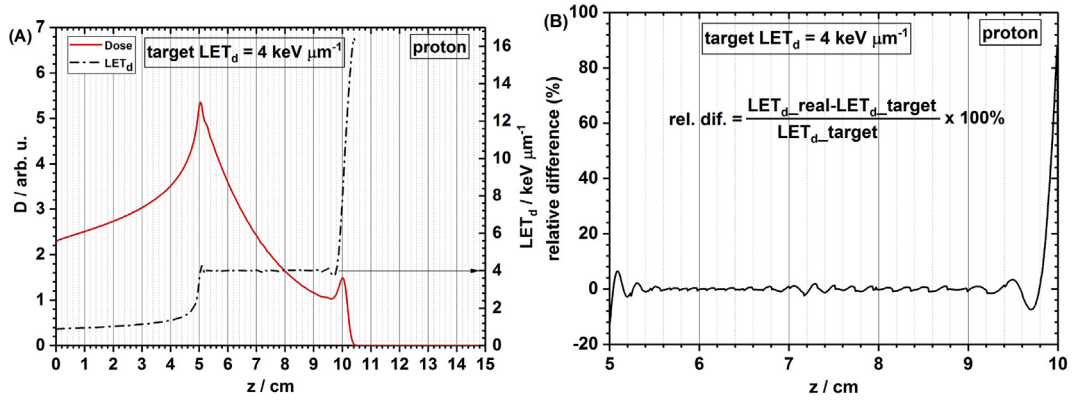

Fig. 8. (A) Weights of beams are optimized to deliver a uniform target dose-averaged linear energy transfer (LET$_d$) of 4 keV/μm to the target region from 5 to 10 cm. The optimization region ranges from 4.5 to 10.5 cm to maintain a small fluctuation of LET$_d$ within the target region. (B) Relative difference between the real LET$_d$ after the optimization procedure and the expected target LET$_d$ (4 keV/μm). The relative difference within the central area, i.e., from 5.5 to 9.5 cm, is between −2.5% and 3.5%. However, the relative difference can be as high as -17% and 88% at the lower and higher boundaries.

from 5 to 10 cm, but we can still see the large variation at the lower and higher boundary of the optimization target from 4.5 to 10.5 cm as expected. The relative difference within the irradiation target region is between −2.5% and 2.0%.

Then, we increased the expected LET$_d$ within the irradiation target region to be 8 keV/μm. However, the optimization results showed that the optimizer could not find appropriate solutions for the beam weights. In Fig. 10A, the real LET$_d$ within the target region is about 6.2 keV/μm. The relative difference in Fig. 10B shows that the largest deviation can be approximately −25%. This observation can be qualitatively explained using the LET$_d$ results in Fig. 3B where the LET$_d$ ranges from 1.8 to 8.5 keV/μm from 5 to 10 cm. The current expected target LET$_d$ value of 8.0 keV/μm is very close to the largest value of 8.5 keV/μm at the higher boundary. A reasonable target LET$_d$ value should not be too far away from the middle value of the highest and the lowest LET$_d$. It is not practical to perform the radiobiology experiments using the results in Fig. 10A because the dose varies largely across the irradiation target, i.e., from 100 Gy to close to 0 with the dose of 2 Gy at the middle point of the target.

4. Discussion

The optimization algorithms presented in the current study can generate high-accuracy optimized results of the specified physical quantity within the target. For the dose optimization results presented in the current study, the relative difference for most spatial locations was within ± 1.0%. The relative difference for ^{12}C beams was the smallest because all Bragg peaks were broadened by the ripple filter, whereas for ^{4}He and proton beams, no ripple filter was applied to broaden the Bragg peaks. When the optimization boundaries are consistent with the boundaries of the target region, the largest fluctuations of the relative difference occur at the boundaries of the target region.

After extending the optimization boundaries outside of the irradiation target region, we found that the relative difference had much smaller fluctuations within the irradiation target. When the expected target LET$_d$ is a reasonable value, e.g., 4 keV/μm, the relative difference within the target can be within ± 2.0%. The LET$_d$ of proton beams is an absolute physical quantity and has a limited range of values, as shown in Fig. 1B; therefore, the optimizer may not find appropriate solutions for the beam weights if the specified target LET$_d$ is too high or too low, such as in the case with a high target LET$_d$ of 8 keV/μm.

These optimization results provide a useful beam delivery strategy to investigate biological effects using scanned beams with different spatial distributions of a specified physical quantity, e.g., dose for proton and ion beams and LET$_d$ for proton beams. For example, we can design a multi-step radiation device (a range shifter) with different step thicknesses, each of which corresponds to a specified depth in the water phantom along the distribution curve of a physical quantity, e.g., a dose SOBP curve. The principle of this experimental design, using a high-throughput irradiation strategy for different ion species with mono-energetic beams, was described in our previous study [30,42]. If we place the 12 columns of a 96-well cell culture plate on top of this multi-

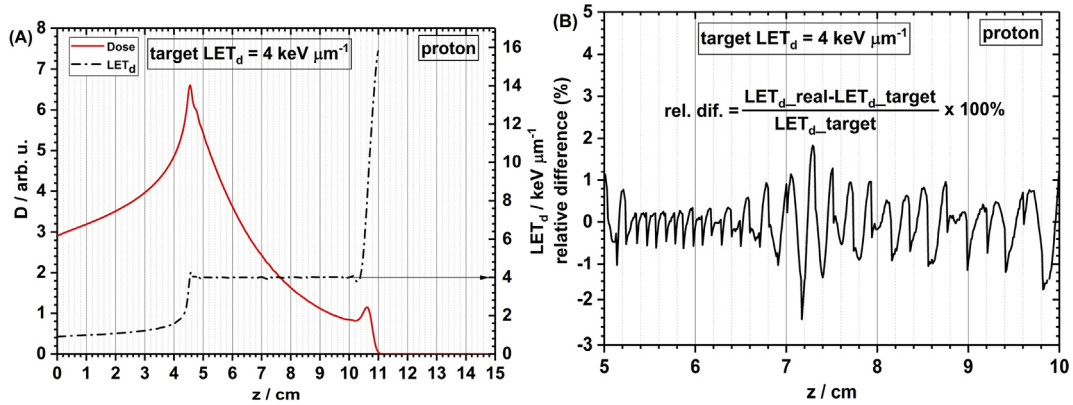

Fig. 9. (A) Weights of beams are optimized to deliver a uniform dose-averaged linear energy transfer (LET$_d$) of 4 keV/μm to the region from 5 to 10 cm. The optimization target region ranges from 4.5 to 10.5 cm to maintain a small fluctuation of LET$_d$ in the irradiation target region from 5 to 10 cm. (B) Relative difference between the real LET$_d$ after the optimization procedure and the expected target LET$_d$ (4 keV/μm). The relative difference within the irradiation target region is between −2.5% and 2.0%.

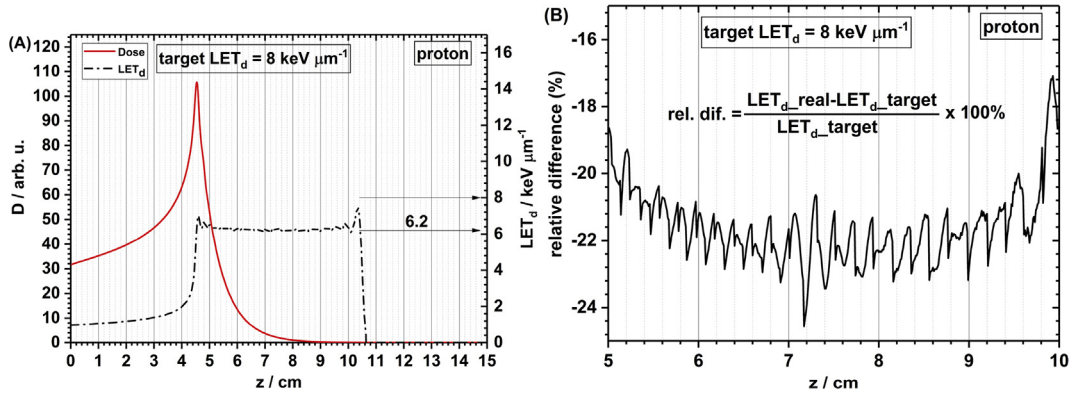

Fig. 10. (A) We set the target dose-averaged linear energy transfer (LET$_d$) to be 8 keV/μm, but the optimizer could not find appropriate solutions of the weights of beamlets. Therefore, the real LET$_d$ value and the expected LET$_d$ value can have large relative differences, as shown in (B).

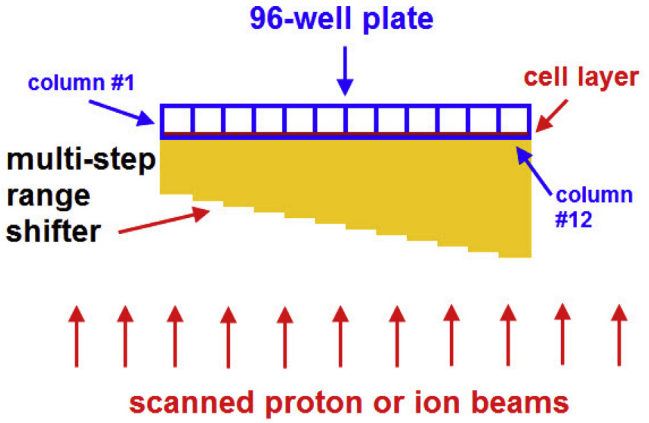

Fig. 11. High-throughput experimental setup for using a multi-step range shifter and 96-well plates to investigate the spatial variation of biological effects of protons or heavy ions, using scanned beams.

step range shifter, the spatial variation of the biological effect can be sampled at 12 locations in a single irradiation run. This experimental setup is illustrated in Fig. 11.

The 12 marked locations in Fig. 3B can be used to explain the principle of this experimental design, in which we place the 10 middle columns of the 96-well plate within the SOBP, the first column proximal and the last column distal to the SOBP. The combined use of a multi-step range shifter and 96-well cell culture plates can provide a high-efficiency way to investigate the spatial variation of biological effects, e.g., clonogenic cell survival or DNA damage, along the beam path. In addition, the thickness of each step can be customized to match any desired depth in the water phantom. We can use a high-accuracy milling machine or three-dimensional printer to fabricate the range shifter so that biological data with a high spatial resolution can be obtained.

5. Conclusions

In the current work, we have developed an easy-to-implement optimization strategy to deliver a desired spatial distribution of the physical quantity of interest to the target region, by combining Monte Carlo simulation techniques with the Python programming language. We have demonstrated the feasibility and flexibility of the physical quantity optimization method for different ions and different spatial distributions of the specified physical quantity. Our optimization algorithms can generate highly accurate solutions for the beam weights, and the generated beam delivery strategy can be used in next-step radiobiology experiments to rapidly obtain the spatial distribution of the biological effects of different ions by combining high-throughput cell culture methods with a multi-step range shifter.

The one-dimensional optimization algorithms developed in the current study can be extended to two or three dimensions if the corresponding physical data are available. The methodology developed for physical quantity optimization can be conveniently extended to perform RBE-weighted dose optimization procedures if appropriate biophysical models are involved in the iteration process for solving the beam weights. Biological dose optimization methods and results for different ions will be reported elsewhere.

6. Declarations of interest

None.

Acknowledgments

This work was supported by the National Cancer Institute – United States [Grant No. U19 CA021239] and the Research Seed Funding Initiative Award from the American Association of Physicists in Medicine – United States.

References

[1] Particle Therapy Co-Operative Group; 2017.
[2] ICRU. Prescrbing, recording, and reporting proton-beam therapy (ICRU Report 78). J ICRU. 2007; 7: NP.
[3] Yock TI, Yeap BY, Ebb DH, Weyman E, Eaton BR, Sherry NA, et al. Long-term toxic effects of proton radiotherapy for paediatric medulloblastoma: a phase 2 single-arm study. Lancet Oncol 2016;17:287–98.
[4] Eaton BR, Esiashvili N, Kim S, Weyman EA, Thornton LT, Mazewski C, et al. Clinical outcomes among children with standard-risk medulloblastoma treated with proton and photon radiation therapy: a comparison of disease control and overall survival. Int J Radiat Oncol Biol Phys 2016;94:133–8.
[5] Marx V. Cancer treatment: sharp shooters. Nature 2014;508:133–8.
[6] Flanz J, Bortfeld T. Evolution of technology to optimize the delivery of proton therapy: the third generation. Seminars in Radiation Oncology. Elsevier; 2013. p. 142–8.
[7] Mailhot Vega RB, Kim J, Bussière M, Hattangadi J, Hollander A, Michalski J, et al. Cost effectiveness of proton therapy compared with photon therapy in the management of pediatric medulloblastoma. Cancer 2013;119:4299–307.
[8] Das IJ, Paganetti H. Medicine AAoPi. Principles and practice of proton beam therapy. Medical Physics Publishing; 2015.
[9] Paganetti H. Proton therapy physics. CRC Press; 2011.
[10] Krämer M, Scifoni E, Schmitz F, Sokol O, Durante M. Overview of recent advances in treatment planning for ion beam radiotherapy. Eur Phys J D 2014;68:306.
[11] Krämer M, Jäkel O, Haberer T, Kraft G, Schardt D, Weber U. Treatment planning for heavy-ion radiotherapy: physical beam model and dose optimization. Phys Med Biol 2000;45:3299.
[12] Loeffler JS, Durante M. Charged particle therapy—optimization, challenges and future directions. Nat Rev Clin Oncol 2013;10:411.
[13] Krämer M, Scholz M. Treatment planning for heavy-ion radiotherapy: calculation and optimization of biologically effective dose. Phys Med Biol 2000;45:3319.
[14] Combs SE, Jäkel O, Haberer T, Debus J. Particle therapy at the Heidelberg Ion Therapy Center (HIT)–integrated research-driven university-hospital-based radiation oncology service in Heidelberg, Germany. Radiother Oncol 2010;95:41–4.
[15] Lomax A. Intensity modulation methods for proton radiotherapy. Phys Med Biol

1999;44:185.
[16] Jette D, Chen W. Creating a spread-out Bragg peak in proton beams. Phys Med Biol 2011;56:N131.
[17] Schell S, Wilkens JJ. Modifying proton fluence spectra to generate spread-out Bragg peaks with laser accelerated proton beams. Phys Med Biol 2009;54:N459–66.
[18] Lu HM, Kooy H. Optimization of current modulation function for proton spread-out Bragg peak fields. Med Phys 2006;33:1281–7.
[19] Bortfeld T, Schlegel W. An analytical approximation of depth-dose distributions for therapeutic proton beams. Phys Med Biol 1996;41:1331–9.
[20] Bortfeld T. An analytical approximation of the Bragg curve for therapeutic proton beams. Med Phys 1997;24:2024–33.
[21] Dias MF, Riboldi M, Seco J, Castelhano I, Pella A, Mirandola A, et al. Scan path optimization with/without clustering for active beam delivery in charged particle therapy. Phys Med Eur J Med Phys 2015;31:130–6.
[22] Austin AM, Douglass MJ, Nguyen GT, Penfold SN. A radiobiological Markov simulation tool for aiding decision making in proton therapy referral. Phys Med Eur J Med Phys 2017;44:72–82.
[23] Kanematsu N. Dose calculation algorithm of fast fine-heterogeneity correction for heavy charged particle radiotherapy. Phys Med: Eur J Med Phys 2011;27:97–102.
[24] Trott K-R. Special radiobiological features of second cancer risk after particle radiotherapy. Physica Med 2017;42:221–7.
[25] Bassler N, Jäkel O, Søndergaard CS, Petersen JB. Dose-and LET-painting with particle therapy. Acta Oncol 2010;49:1170–6.
[26] Bassler N, Toftegaard J, Lühr A, Sørensen BS, Scifoni E, Krämer M, et al. LET-painting increases tumour control probability in hypoxic tumours. Acta Oncol 2014;53:25–32.
[27] Agostinelli SAJ, Amako K, Apostolakis J, Araujo H, Arce P, Asai M, et al. Geant4—a simulation toolkit. Nucl Instrum Methods Phys Res, Sect A 2003;506:250–303.
[28] Allison J, Amako K, Apostolakis J, Arce P, Asai M, Aso T, et al. Recent developments in Geant4. Nucl Instrum Methods Phys Res, Sect A 2016;835:186–225.
[29] Taleei R, Guan F, Peeler C, Bronk L, Patel D, Mirkovic D, et al. Monte Carlo simulations of 3He ion physical characteristics in a water phantom and evaluation of radiobiological effectiveness. Med Phys 2016;43:761–76.
[30] Patel D, Bronk L, Guan F, Peeler CR, Brons S, Dokic I, et al. Optimization of Monte Carlo particle transport parameters and validation of a novel high throughput experimental setup to measure the biological effects of particle beams. Med Phys 2017;44:6061–73.
[31] Berger MJ. ESTAR, PSTAR and ASTAR: Computer programs for calculating stopping powers and ranges for electrons, protons and helium ions; 1995.
[32] Sigmund P, Schinner A, Paul H. Errata and addenda for ICRU report 73, stopping of ions heavier than helium. ICRU J 2009;5(1).
[33] Brun R, Rademakers F. ROOT — An object oriented data analysis framework. Nucl Instrum Methods Phys Res, Sect A 1997;389:81–6.
[34] Levenberg K. A method for the solution of certain non-linear problems in least squares. Q Appl Math 1944;2:164–8.
[35] Giantsoudi D, Grassberger C, Craft D, Niemierko A, Trofimov A, Paganetti H. Linear energy transfer-guided optimization in intensity modulated proton therapy: feasibility study and clinical potential. Int J Radiat Oncol Biol Phys 2013;87:216–22.
[36] Carabe-Fernandez A, Dale RG, Jones B. The incorporation of the concept of minimum RBE (RBE min) into the linear-quadratic model and the potential for improved radiobiological analysis of high-LET treatments. Int J Radiat Biol 2007;83:27–39.
[37] McNamara AL, Schuemann J, Paganetti H. A phenomenological relative biological effectiveness (RBE) model for proton therapy based on all published in vitro cell survival data. Phys Med Biol 2015;60:8399–416.
[38] Cao W, Khabazian A, Yepes PP, Lim G, Poenisch F, Grosshans DR, et al. Linear energy transfer incorporated intensity modulated proton therapy optimization. Phys Med Biol 2017;63:015013.
[39] ICRU. Fundamental quantities and units for ionizing radiation (ICRU Report 85). J ICRU. 2011; 11:1–31.
[40] Paganetti H. Proton Therapy Physics. Proton Therapy Physics Series: Series in Medical Physics and Biomedical Engineering, in: Harald Paganetti (ed.), CRC Press, ISBN: 978-1-4398-3644-6; 2011.
[41] Guan F, Peeler C, Bronk L, Geng C, Taleei R, Randeniya S, et al. Analysis of the track- and dose-averaged LET and LET spectra in proton therapy using the geant4 Monte Carlo code. Med Phys 2015;42:6234–47.
[42] Guan F, Bronk L, Titt U, Lin SH, Mirkovic D, Kerr MD, et al. Spatial mapping of the biologic effectiveness of scanned particle beams: towards biologically optimized particle therapy. Sci Rep 2015;5:9850.